Summer snow on Arctic sea ice modulated by the Arctic Oscillation

Melinda A. Webster [1] ✉, Aku Riihelä [2], Sahra Kacimi[3], Thomas J. Ballinger[4], Edward Blanchard-Wrigglesworth [5], Chelsea L. Parker[6,7] & Linette Boisvert[7]

Since the 1970s, Arctic sea ice has undergone unprecedented change, becoming thinner, less extensive and less resilient to summer melt. Snow's high albedo greatly reduces solar absorption in sea ice and the upper ocean, which mitigates sea–ice melt and ocean warming. However, the drivers of summertime snow depth variability are unknown. The Arctic Oscillation is a mode of natural climate variability, influencing Arctic snowfall and air temperatures. Thus, it may affect summertime snow conditions on Arctic sea ice. Here we examine the role of the Arctic Oscillation in summer snow depth variability on Arctic sea ice in 1980–2020 using atmospheric reanalysis, snow modelling and satellite data. The positive phase leads to greater snow accumulation, ranging up to ~4.5 cm near the North Pole, and higher surface albedo in summer. There are more intense, frequent Arctic cyclones, cooler temperatures aloft and greater snowfall relative to negative and neutral phases; these conditions facilitate a more persistent summer snow cover, which may lessen sea-ice melt and ocean warming. The Arctic Oscillation influence on summertime snow weakens after 2007, which suggests that future warming and Arctic sea-ice loss might modify the relationship between the Arctic Oscillation and snow on Arctic sea ice.

Snow is one of the most reflective[1-3] and insulative[4-6] natural materials on Earth. As a consequence, snow on sea ice is an integral part of the sea-ice and climate systems[7,8]. Understanding the mechanisms that control the magnitude and timing of snow accumulation is of critical importance for reliably predicting sea-ice conditions. However, there are challenges in accurately predicting snow conditions on sea ice. Because snow is tightly coupled to sea-ice and atmospheric conditions[9,10], the snow processes that dominate changes in space and time. There is generally good understanding of the physical processes that affect the spatial distribution of snow, but acute knowledge gaps exist on the drivers of snow's temporal variability.

For snow distribution on the pan-Arctic scale, the timing of sea-ice formation is key. Later ice formation reduces the amount of time that snowfall can accumulate on sea ice, leading to a thinner snowpack[11,12]. This relationship is most evident in the pan-Arctic gradient in spring snow depth, from the relatively thin snow (15–25 cm) on seasonal ice in the Chukchi Sea to the thicker snow (30–45 cm) on multiyear ice in the Lincoln Sea[10,13-16]. There are regional exceptions to this spatial gradient in snow depth, however. In the North Atlantic sector, considerably deeper snowpacks (40+ cm averages) can occur despite much of the sea ice being seasonal (ref. 17 and references therein). The deeper snow in this region is attributable to the position of the North Atlantic storm track, which brings frequent, heavy snowfall throughout the sea-ice growth period[18]. It is the interplay between the timing of snowfall and the presence of sea ice that dictates the regional distribution of snow on Arctic sea ice in autumn–spring.

[1]Polar Science Center, Applied Physics Laboratory, University of Washington, Seattle, WA, USA. [2]Meteorological Research, Finnish Meteorological Institute, Helsinki, Finland. [3]Jet Propulsion Laboratory, California Institute of Technology, Pasadena, CA, USA. [4]International Arctic Research Center, University of Alaska Fairbanks, Fairbanks, AK, USA. [5]Department of Atmospheric Sciences, University of Washington, Seattle, WA, USA. [6]Earth System Science Interdisciplinary Center, University of Maryland, College Park, MD, USA. [7]Cryospheric Sciences Laboratory, NASA Goddard Space Flight Center, Greenbelt, MD, USA. ✉e-mail: melindaw@uw.edu
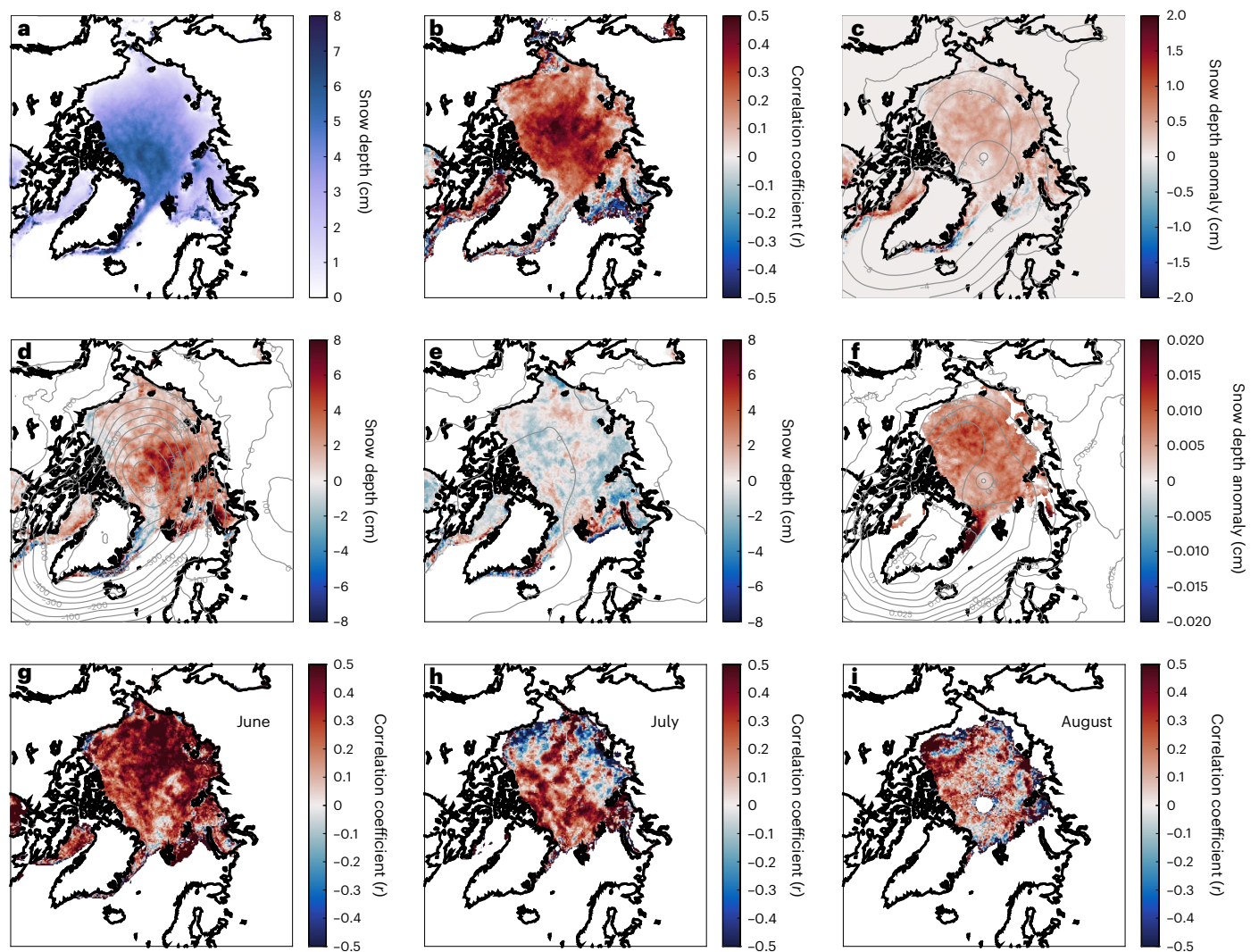
Fig. 1 | The relationship between snow depth on Arctic sea ice and the Arctic Oscillation. a–f, The June–August mean for 1980–2020 in snow depth (**a**), the correlation between snow depth anomalies and the Arctic Oscillation (AO) (**b**), snow depth anomalies regressed onto the AO index (**c**), the linear response (composite difference) in snow depth anomalies to the AO (**d**), the nonlinear response (composite sum) in snow depth anomalies to the AO (**e**) and snow depth anomalies regressed onto the first principal component of snow depth (**f**). Correlation coefficients between anomalies in snow depth and blue-sky surface albedo in June (**g**), July (**h**) and August (**i**) for areas with at least 80% sea-ice concentration. The light grey contours in **c–f** are the corresponding results using 1,000 hPa geopotential height anomalies.

Regarding large-scale temporal variability, relatively little is understood about snow on Arctic sea ice. This is in large part due to limited, routine sampling. Historical observations[13,19] give the first long-term time series of snow on Arctic sea ice spanning 1954–1991. The temporal variability is presented as the standard deviation of snow depth anomalies from transect measurements, giving an ~6-cm value for springtime conditions[13]. Because the measurements originated from different drifting ice floes, the variability represents a combination of interannual variability, local-scale heterogeneity and large-scale geographic differences. These measurements are largely limited to the autumn–spring seasons, as sampling ceased during the summer if snow covered less than 50% of the transect line or was less than 5-cm deep[19]. Thus, a substantial knowledge gap exists on the drivers of summertime snow depth variability on Arctic sea ice.

In this study, we aim to remedy this knowledge gap by investigating the linkages between snow on Arctic sea ice and atmospheric variability. We examined the role of the Arctic Oscillation (AO), the dominant atmospheric mode of natural climate variability in the Arctic[20], in snow conditions on Arctic sea ice. Our focus is the summer melt season, a

period in which the presence of snow has a large albedo effect on solar absorption in sea ice[21–24] and, consequently, surface melt.

Summer snow depth variability and albedo

The AO played a large role in summer snow depth variability on Arctic sea ice in 1980–2020. We found that the summertime snow depth anomalies and their leading pattern (first principal component) were strongly related (95% significance) to the AO in the central Arctic (Fig. 1b,c,f and corresponding maps with statistical significance in Extended Data Fig. 1). The linear response (composite difference) of snow to the AO was stronger than that of the nonlinear response (composite sum) (Fig. 1d,e), further indicating that, during positive AO summers (June–August average), there is deeper snow on Arctic sea ice. For context, only ~0.5 cm (2 cm) of fine-grained (coarse-grained) snow is needed to reflect nearly 80% of incoming solar radiation[1,25,26]. During positive AO summers, there is up to ~4.5 cm more snow accumulation near the North Pole relative to neutral AO conditions. Thus, it can be expected that such variability can greatly influence the surface albedo of Arctic sea ice in summer.
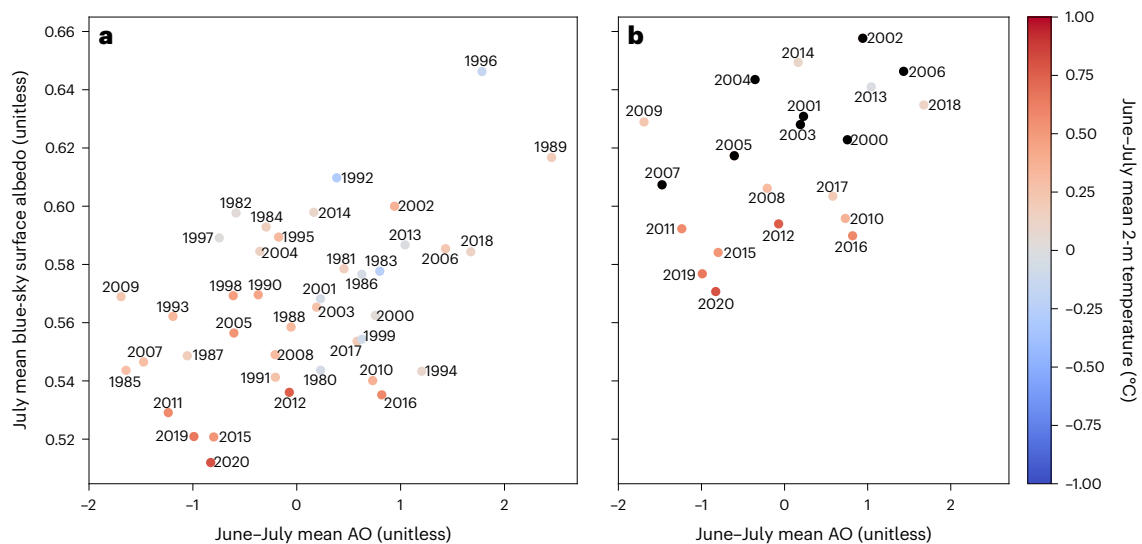
Fig. 2 | The relationship between surface albedo and the Arctic Oscillation. **a,b**, The mean July blue-sky albedo from satellite observations over the continuous (sea-ice concentrations greater than 80%) sea-ice domain of the Arctic Ocean (y axis) against the June–July mean Arctic Oscillation (AO) index for 1980–2020 (**a**) and 2000–2020 (**b**) with a correction for mean albedo effect of melt ponds. Marker colour indicates mean June–July 2 m air temperature of areas poleward of 75° N from ERA5 reanalysis. In **b**, the years 2000–2007, before the weakening of the snowy AO response, are highlighted in black. Note that the temperatures are the same for points between **a** and **b**.

We, therefore, evaluated the relationship between summer snow accumulation, surface albedo and the AO. The variability in snow depth and blue-sky surface albedo are strongly correlated in most of the Arctic in June (Fig. 1g). The exception to this is in the Greenland and Lincoln seas, which tend to have the deepest snowpack on Arctic sea ice[10,13]. Thus, variations in the thickness of deep snow, which already exceeds the snow optical thickness, will not affect the surface albedo[2]. In July, statistically significant correlations are concentrated north of 75° N and in the Kara Sea (Fig. 1h), whereas, in August, they are concentrated in the peripheral seas (Fig. 1i). The spatial pattern in August is notable in the context of freeze-up timing, which we found to be significantly correlated with August snow depth variability (below).

To separate the possible effects of seasonal ice coverage on the albedo results, we investigated the relationship between albedo variability and the AO in the continuous sea-ice zone, following ref. 27. We found that positive AO indices in June–July correlate with higher mean surface albedos in the continuous sea-ice zone in July (Fig. 2a). This is consistent with the preceding finding of a deeper, more expansive summer snowpack on sea ice during the positive AO phase. The AO index and surface albedo are significantly correlated ($r = 0.49$, $P = 0.001$). The low correlation may be due to several factors, including the presence of melt ponds, variations in ice coverage, limited sampling during the earlier satellite era, a negligible albedo effect over pre-existing deep snow and others.

To explore the albedo effect of melt ponds, which have an albedo of 0.12–0.32 (ref. 3), we analysed the 2000–2020 period using available, independent satellite retrievals of melt pond coverage (Fig. 2b). After correcting for mean melt pond albedo effects, the relationship between surface albedo and the AO remains noisy ($r = 0.46$) but statistically significant ($P = 0.030$). This suggests that other factors, such as small variations in sea-ice coverage and, thus, open leads (albedo of 0.07)[28], may have a larger effect on the average July surface albedo than interannual melt pond variability. The increasingly warm summers of the Arctic Ocean (Fig. 2b) are altering the reflective properties of the snow and sea-ice covers and increasing the proportion of liquid precipitation[29]. Both effects will further decrease surface albedo and weaken the correlation.

Melt onset, sea-ice conditions and remnant snow

Snow depth variability during the melt season is influenced by many time-varying physical processes. For example, the timing of melt onset could influence summer snow depth variability by way of a positive albedo feedback. As snow melts, snow grains coarsen, which reduces the reflectivity and increases the transmittance, thereby increasing solar absorption within the snowpack[2]. We found that the relationship between melt onset timing and snow depth variability was weak and not statistically significant when averaged over June–August in 1980–2020 (Fig. 3a–c and corresponding maps with statistical significance in Extended Data Fig. 2). However, for June only, the timing of melt onset and snow depth variability were strongly correlated in much of the eastern and central Arctic (Fig. 3a). Melt onset was strongly correlated to the AO, where, during positive AO summers, the eastern and central Arctic tended to have later melt onset than in negative AO summers. In July and August (Fig. 3b,c), no significant correlations between melt onset and snow depth variability were found, which indicates that melt onset has a short-lived effect on snow depth variability during the melt season.

Sea ice is a platform onto which snow accumulates. Accordingly, sea-ice coverage could affect summer snow depth variability across the Arctic. During the early melt season (June), the variability in June sea-ice coverage significantly explains 19% of the snow depth variance in areas with 95% statistical significance (Fig. 3d and Extended Data Fig. 3d). These areas are concentrated in the peripheral seas (Extended Data Fig. 3d). Sea-ice concentrations from earlier months have no statistically significant relationship with snow depth variability for the remainder of the melt season (Extended Data Fig. 3), which suggests no lag effect between prior months' ice coverage and subsequent months' snow conditions. In July, the relationship between sea-ice concentration and snow depth was weakest. In August, sea-ice concentrations play a significant role in August snow depth variability in most peripheral seas (Fig. 3c and Extended Data Fig. 3l). This relationship partly results from the timing of sea-ice freeze up, which can occur in August (Extended Data Fig. 4a).

As observed in the western Arctic[12], earlier sea-ice freeze up may allow more total snowfall to accumulate, creating a deeper snowpack. Deeper snow requires more energy to completely melt. Consequently,
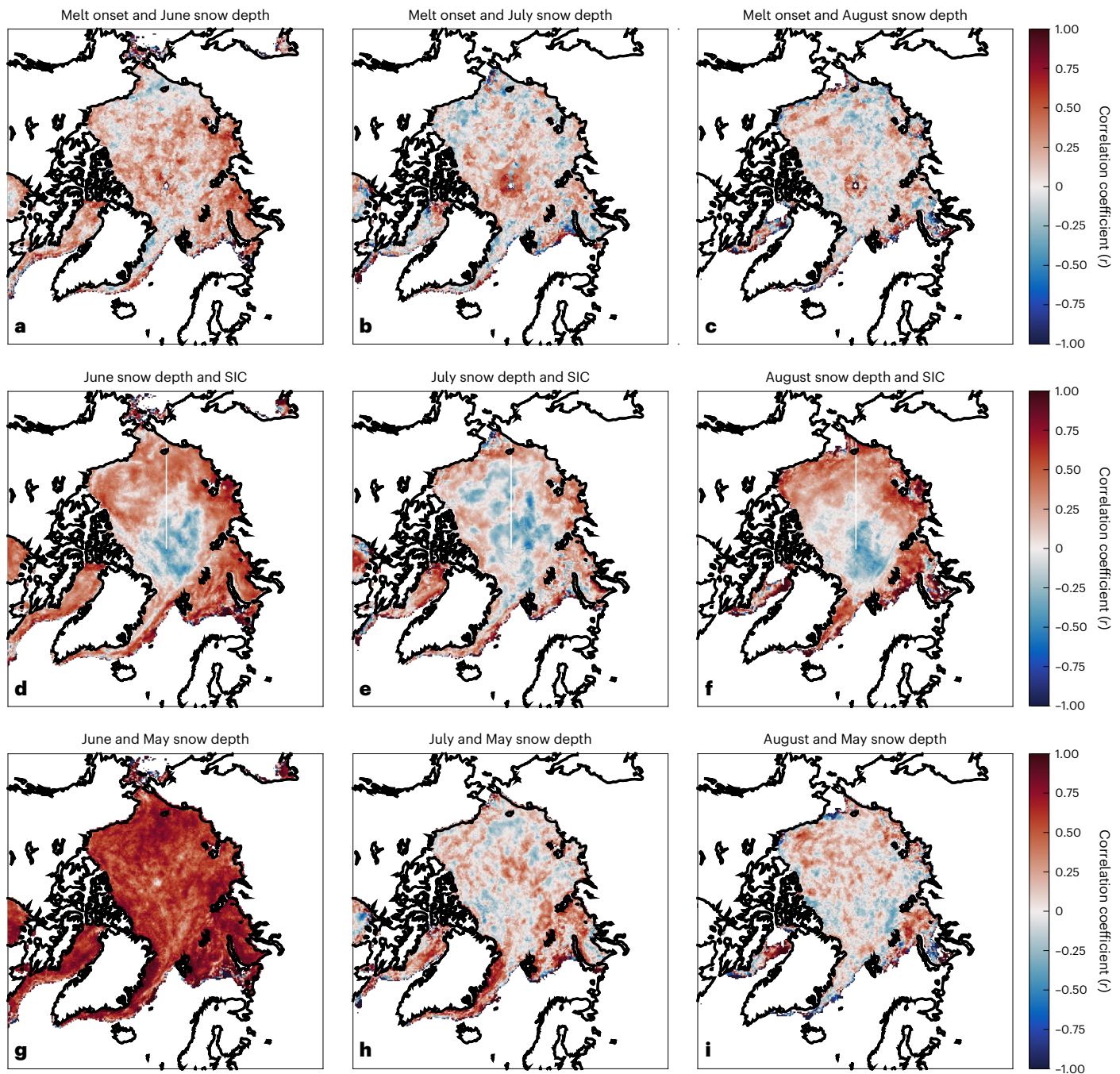
Fig. 3 | The relationships between snow depth variability, melt onset, sea-ice coverage and remnant snow. a–c, Correlation coefficients of 1980–2020 anomalies between the date of melt onset and June (**a**), July (**b**) and August (**c**) snow depths. **d–f**, Snow depths and sea ice concentration (SIC) for June (**d**), July (**e**) and August (**f**). **g–i**, May snow depths and June (**g**), July (**h**) and August (**i**) snow depths. An equivalent figure with 95% statistical significance is available as Extended Data Fig. 3.

the previous year's freeze-up date could affect the following summer's snow depth conditions. We found that the timing of sea-ice freeze up explains 13% of the variance in June snow depth variability in the Kara, E. Laptev, E. Siberian and Chukchi seas. From July onward, the timing of the previous year's freeze up had a negligible effect on snow depth variability (Extended Data Fig. 4b–d). This suggests that the effects of freeze-up timing on snow depth variability may propagate into the early melt season in regions with seasonal ice, but the effects are short-lived.

Remnant snow, or snow that persists from preceding months, plays an important role in snow depth variability during the early melt

season (Fig. 3g–i). Remnant snow from April and May significantly contributes 30% and 74%, respectively, to the snow depth variability in June (Extended Data Fig. 2d–f). In July, remnant snow from June explains 22% of the snow depth variability on average. Snow depths in April–May have the lowest contribution (11%) to August snow depth variability, albeit with no statistical significance. In short, snow depths from late winter, spring and early summer strongly covary, but their impact on mid and late summer snow depth progressively weakens. Sea-ice drift may complicate the causal inferences about remnant snow and summer snow variability. During June–August, Arctic sea-ice drifts ~6 km per day on average[30]. This equates to an ~550-km distance from early June
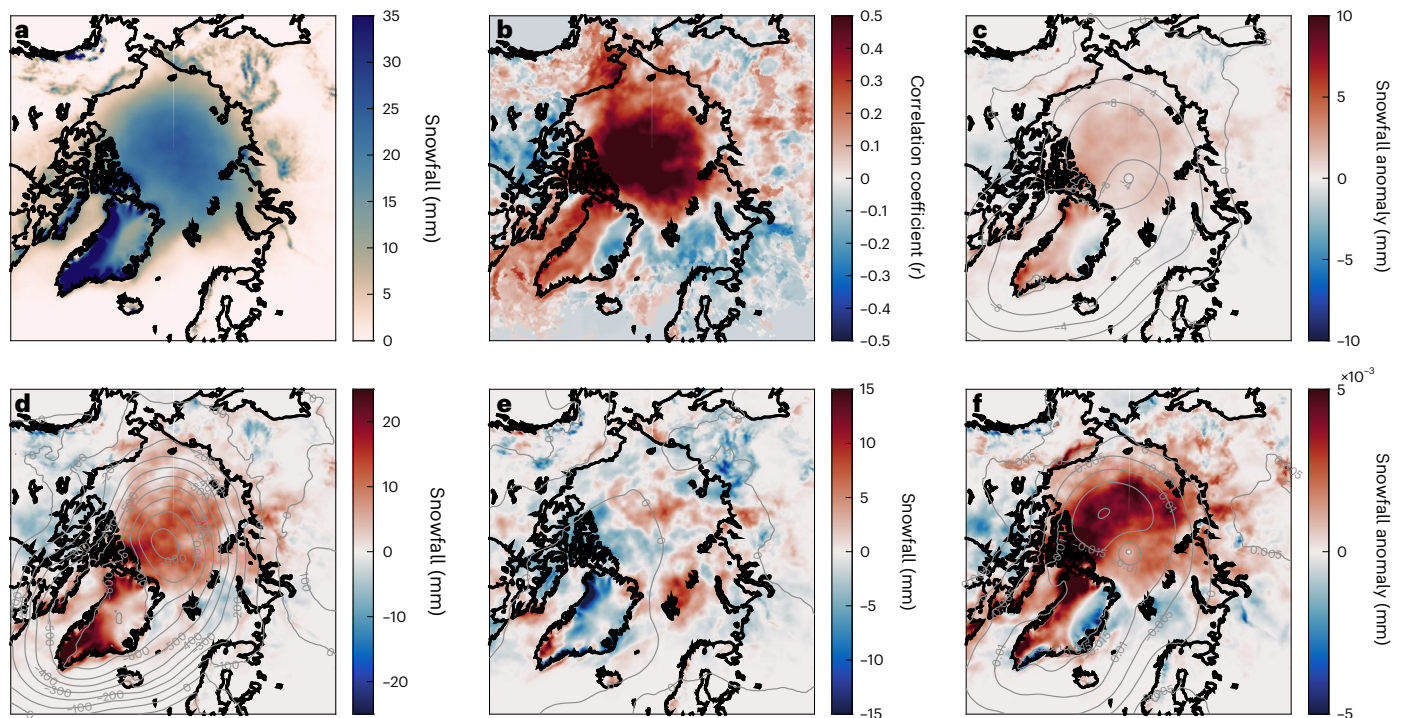
Fig. 4 | The relationship between snowfall and the Arctic Oscillation.
a–**f**, The June–August mean for 1980–2020 in snowfall (**a**), the correlation between snowfall anomalies and the Arctic Oscillation (AO) (**b**), snowfall anomalies regressed onto the AO index (**c**), the linear response (composite difference) in snowfall anomalies to the AO (**d**), the nonlinear response (composite sum) in snowfall anomalies to the AO (**e**) and snowfall anomalies regressed onto the first principal component of snowfall (**f**). The light grey contours in **c**–**f** are the corresponding results using 1,000 hPa geopotential height anomalies.

to late August. Hence, snow depths in one region in early summer may not strongly correlate with those in the same region in late summer. The weaker correlations in snow depths between May and later months may be influenced by such drift effects (Fig. 3g–i).

To summarize, the influence of melt onset and remnant spring snow on summer snow depth variability appears to be largely limited to June. This suggests that snowfall and air temperature, rather than sea-ice state and pre-existing snow conditions, play a larger role in snow depth variability during the mid-to-late summer melt season, which we demonstrate next.

Atmospheric conditions

The positive phase of the AO in summer facilitates enhanced Arctic snowfall by way of cooler temperatures aloft and a more active, northerly Atlantic storm track (Extended Data Fig. 5). The leading pattern of variability in summer snowfall is strongly related to the AO (Fig. 4c,d,f). During positive AO summers, there are cooler temperatures at the 850-hPa level, which promotes higher snowfall-to-total precipitation ratios (Fig. 5). Although more rainfall and more total precipitation occur during positive AO summers, snowfall dominates the precipitation increase. In particular, snowfall in the central Arctic, north of Alaska, Lincoln Sea and the northern Canadian Arctic Archipelago is most strongly (95% significance) correlated with the AO (Fig. 4b). During positive AO summers, there is ~5 mm more snow water equivalent on average, which is ~2.5 cm of snow accumulation assuming a fresh snowfall density of 0.2 g cm^{-3} (ref. [19]).

Cyclones are the key mechanism for establishing the snowpack over Arctic sea ice in autumn–spring[18], and in June–August, they are associated with cooler conditions and greater snowfall[31]. We, therefore, explored the relationship between the AO and cyclone activity to determine whether cyclones' precipitation plays an important role in summer snow depth variability. We found that more cyclones penetrate

deeper into the Arctic during positive AO summers, as indicated by the high significant correlations and strong linear response (Fig. 6b,d). This result agrees with previous studies investigating Arctic cyclone activity and the Northern Atlantic Oscillation and AO[32–35]. However, we found a strong negative nonlinear response north of Greenland and the Canadian Arctic Archipelago (Fig. 6e), which suggests that fewer cyclones may occur in that region during extreme positive and negative AO summers.

On average, cyclones were more intense during positive AO summers (Extended Data Fig. 7); minimum sea level pressures (SLPs) were ~3 hPa and ~8 hPa lower relative to neutral and negative AO phases, respectively. This, together with cooler temperatures aloft (Fig. 5a–c), probably contributed to greater snowfall in the central Arctic during positive AO summers in 1980–2020. Indeed, there is ~1 mm of additional water equivalent from enhanced cyclone snowfall during positive AO summers. Collectively, these results demonstrate that a positive AO contributes to more frequent summer snow accumulation on Arctic sea ice by way of enhanced storm activity and snowfall.

In addition to enhanced snowfall, freezing conditions at the sea-ice surface can allow snow to persist longer during summer. Accordingly, we evaluated 2 m air temperatures and found weak, inverse correlations with the AO. This suggests that during positive AO summers, there could be cooler surface air temperatures. However, statistically significant correlations were limited to the central Arctic (Extended Data Fig. 1). The leading pattern of variability, as well as the linear and nonlinear responses, are within the noise of the 2 m air temperature time series based on a Z-test (Extended Data Fig. 6).

We performed a monthly lag analysis to explore the possibility of preconditioning effects of atmospheric variability on snow depth variability. The zero-month lag for 2 m temperatures, snowfall and cyclones yielded the highest and only statistically significant (95%) correlation. This suggests that the AO affects storm tracks, precipitation
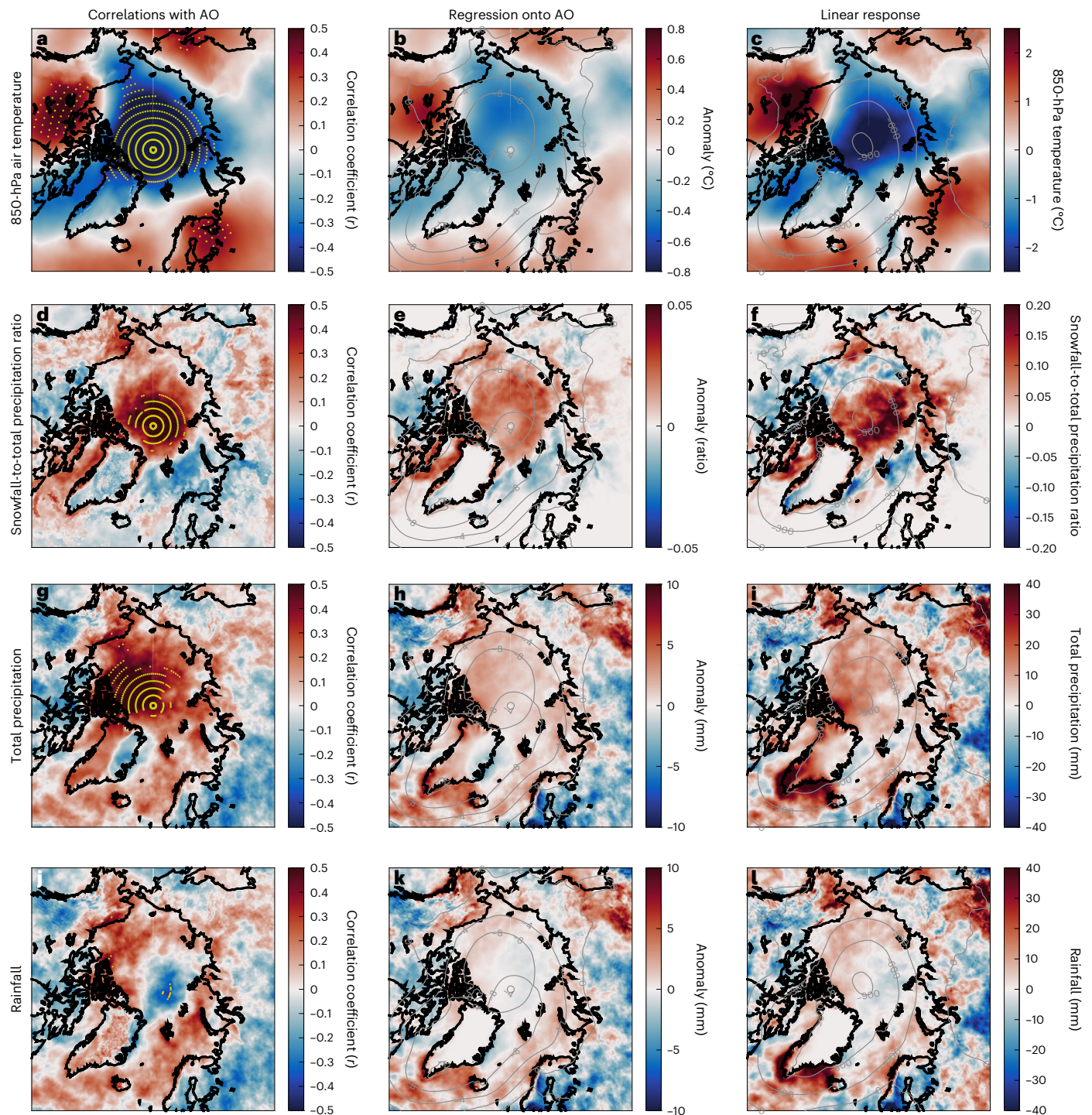
Fig. 5 | The relationship between 850-hPa air temperature, snowfall-to-total precipitation ratio, total precipitation, rainfall and the Arctic Oscillation. **a–l**, The June–August results for 1980–2020 of column 1 correlations with the Arctic Oscillation (AO), column 2 regressions onto the AO and column 3 linear response (composite difference) for 850-hPa air temperature (**a–c**), snowfall-to-total precipitation ratio (**d–f**), total precipitation (**g–i**) and rainfall (**j–l**), computed as the difference between the total precipitation minus snowfall. The yellow dots represent 95% statistical significance in **a**, **d**, **g** and **j**.

and surface temperatures on relatively short timescales and has a near-immediate (but short-lived) effect on snow depth variability during the mid-to-late summer melt season.

Effects of Arctic sea-ice loss

There has been a profound loss of Arctic sea ice since the late 1970s[36]. Given the state change in the Arctic sea-ice cover, we re-examined the relationship between snow depth variability, the AO, sea ice and

atmospheric variables before and after the breakpoint of 2007 in the June–August sea-ice concentration time series (Extended Data Fig. 8). Post 2007, we found weaker summertime relationships between the AO and snow depth, snowfall and air temperature and cyclone frequency, intensity, 2 m temperature and snowfall. In particular, negative correlations emerged between the AO and snow depth, snowfall and cyclone frequency in the coastal areas of the Pacific sector, albeit, not statistically significant. Interestingly, negative (but not statistically significant)
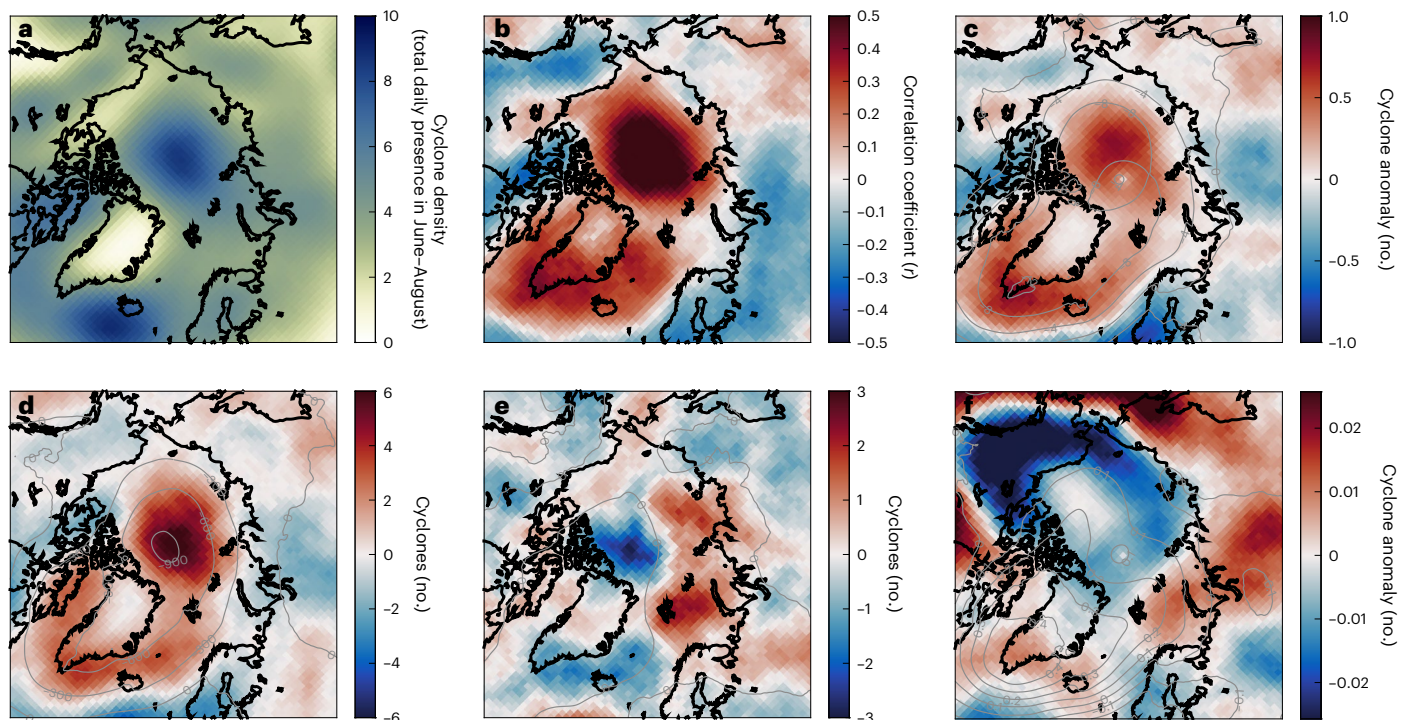
Fig. 6 | The relationship between cyclone activity and the Arctic Oscillation.
a–**f**, The June–August mean for 1980–2020 in the summed daily presence
of cyclones (**a**), the correlation between cyclone anomalies and the Arctic
Oscillation (AO) (**b**), cyclone anomalies regressed onto the AO index (**c**), the
linear response (composite difference) in cyclone anomalies to the AO (**d**), the
nonlinear response (composite sum) in cyclone anomalies to the AO (**e**) and
cyclone anomalies regressed onto the first principal component of cyclones
(**f**). The light grey contours in **c**–**f** are the corresponding results using 1,000 hPa
geopotential height anomalies.

correlations emerged between the AO and sea-ice concentration (SIC)
post 2007. The loss of sea ice may contribute to warmer temperatures,
less snowfall and less snow accumulation during positive AO summers.
Indeed, earlier work[37] found a weakening in Arctic cyclones over the
1979–2009 period, which was attributed to atmospheric warming. We
found no statistically significant trend in cyclone intensity for 1980–
2020, 1980–2006 or 2007–2020, agreeing with recent findings[31]. Note,
care should be taken when interpreting trends in cyclone characteris-
tics, as they are dependent on the algorithm and reanalysis product[38].
Furthermore, the results and statistical significance presented here
should be interpreted with caution considering that the breakpoint
of 2007 gives 14 sample years for the post 2007 period.

Summertime snow and the AO in past and contemporary periods

For 1980–2020, the positive phase of the AO in summer led to cooler
temperatures aloft and enhanced snowfall, which increased snow accu-
mulation on Arctic sea ice and, consequently, raised the surface albedo.
Because our analysis is largely based on reanalysis and model data, we
examined historical and contemporary snow observations from the
North Pole drifting ice stations[39] and ice mass balance buoys[40] for pos-
sible corroborating results. Averaged over June–August, the snow depth
observations from 1962–2017 were positively correlated with the AO
($r = 0.37$) with 86% statistical significance (Extended Data Fig. 9). While
the result lends supporting evidence of this study's conclusions, the
interpretation of the correlation warrants caution as some years con-
sisted of only one to three-point measurements from different locations.

The relationship between the AO and summertime snow may be
useful for analyses on the preconditioning and predictability of Arctic
sea ice during the melt season. Given that most variables in our analysis
exhibited a strong linear response to the AO in 1980–2020, it is insightful
to consider that during negative AO summers, the opposite phenom-
enon tends to occur: during negative AO summers, there are warmer
temperatures aloft, less snowfall, less snow accumulation and lower
surface albedo, all of which would promote greater surface melt. While
the results presented in this work largely summarize the mean pan-Arctic
response to the AO in summer, there are regional exceptions. Notably,
the Barents Sea experienced enhanced warming during positive AO
summers, which contributed to anomalously low snowfall, anomalously
high rainfall, thinner snow depths and less extensive sea-ice coverage
in that region in 1980–2020. This result underscores the complexity in
atmosphere–ice–ocean interactions across the Arctic.

The influence of the AO on summertime snow weakens after 2007,
which suggests that future warming and Arctic sea-ice loss may modify
the relationship between the AO and snow on Arctic sea ice. We specu-
late the link weakened after 2007 due to the combined effects of the
warming trend in the Arctic[41]. There is less sea-ice coverage[36] to capture
falling snow, and more summer precipitation is coming in the form of
rain rather than snow[29] in the contemporary period. With Arctic sea-ice
loss projected to continue[42,43], it will be especially relevant to revisit this
analysis in future decades to better understand the evolving relationship
between the AO and Arctic snow–sea ice system in a warmer climate.

Online content

Any methods, additional references, Nature Portfolio reporting
summaries, source data, extended data, supplementary informa-
tion, acknowledgements, peer review information; details of author
contributions and competing interests; and statements of data and code
availability are available at https://doi.org/10.1038/s41561-024-01525-y.

References

1. Perovich, D. K., Grenfell, T. C., Light, B. & Hobbs, P. V. Seasonal
   evolution of the albedo of multiyear Arctic sea ice. *J. Geophys.
   Res.* **107**, 8044 (2002).
2. Warren, S. G. Optical properties of ice and snow. *Philos. Trans. R.
   Soc. A* **377**, 20180161 (2019).

3. Light, B. et al. Arctic sea ice albedo: spectral composition, spatial heterogeneity, and temporal evolution observed during the MOSAiC drift. *Elementa Sci. Anthrop.* **10**, 000103 (2022).
4. Sturm, M., Holmgren, J., Konig, M. & Morris, K. The thermal conductivity of seasonal snow. *J. Glaciol.* **43**, 26–41 (1997).
5. Sturm, M., Perovich, D. K. & Holmgren, J. Thermal conductivity and heat transfer through the snow on the ice of the Beaufort Sea. *J. Geophys. Res.* **107**, 8043 (2002).
6. Zhang, T. Influence of the seasonal snow cover on the ground thermal regime: an overview. *Rev. Geophys.* **43**, RG4002 (2005).
7. Ledley, T. S. Snow on sea ice: competing effects in shaping climate. *J. Geophys. Res.* **96**, 17195–17208 (1991).
8. Holland, M. M. et al. The influence of snow on sea ice as assessed from simulations of CESM2. *Cryosphere* https://doi.org/10.5194/tc-2021-174 (2021).
9. Sturm, M. & Massom, R. A. in *Sea Ice* 3rd edn (ed. Thomas, D. N.) 65–109 (Wiley and Blackwell, 2017).
10. Webster, M. et al. Snow in the changing sea-ice systems. *Nat. Clim. Change* **8**, 946–953 (2018).
11. Hezel, P. J., Zhang, X., Bitz, C. M., Kelly, B. P. & Massonnet, F. Projected decline in spring snow depth on Arctic sea ice caused by progressively later autumn open ocean freeze-up this century. *Geophys. Res. Lett.* **39**, L17505 (2012).
12. Webster, M. et al. Interdecadal changes in snow depth on Arctic sea ice. *J. Geophys. Res. Oceans* **119**, 5395–5406 (2014).
13. Warren, S. et al. Snow depth on Arctic sea ice. *J. Clim.* **12**, 1814–1829 (1999).
14. Kwok, R. et al. Airborne surveys of snow depth over Arctic sea ice. *J. Geophys. Res.* **116**, C11018 (2011).
15. Kurtz, N. & Farrell, S. Large-scale surveys of snow depth on Arctic sea ice from Operation IceBridge. *Geophys. Res. Lett.* **38**, L20505 (2011).
16. Blanchard-Wrigglesworth, E., Webster, M., Farrell, S. L. & Bitz, C. Reconstruction of snow on Arctic sea ice. *J. Geophys. Res.* **123**, 3588–3602 (2018).
17. Merkouriadi, I., Cheng, B., Graham, R. M., Rösel, A. & Granskog, M. A. Critical role of snow on sea ice growth in the Atlantic sector of the Arctic Ocean. *Geophys. Res. Lett.* **44**, 10479–10485 (2017).
18. Webster, M., Parker, C., Boisvert, L. & Kwok, R. The role of cyclones in snow accumulation on Arctic sea ice. *Nat. Commun.* **10**, 5285 (2019).
19. Radionov, V. F., Bryazgin, N. N. & Alexandrov, E. I. *The Snow Cover of the Arctic Basin* (Washington Univ. Seattle Applied Physics Lab, 1997).
20. Thompson, D. W. & Wallace, J. M. The Arctic Oscillation signature in the winter-time geopotential height and temperature fields. *Geophys. Res. Lett.* **25**, 1297–1300 (1998).
21. Light, B., Dickinson, S., Perovich, D. K. & Holland, M. M. Evolution of summer Arctic sea ice albedo in CCSM4 simulations: episodic summer snowfall and frozen summers. *J. Geophys. Res. Oceans* **120**, 284–303 (2015).
22. Perovich, D., Polashenski, C., Arntsen, A. & Stwertka, C. Anatomy of a late spring snowfall on sea ice. *Geophys. Res. Lett.* **44**, 2802–2809 (2017).
23. Lim, W.-I., Park, H.-S., Petty, A. A. & Seo, K.-H. The role of summer snowstorms on seasonal Arctic sea ice loss. *J. Geophys. Res. Oceans* **127**, e2021JC018066 (2022).
24. Chapman-Dutton, H. R. & Webster, M. A. The effects of summer snowfall on Arctic sea ice radiative forcing. *J. Geophys. Res. Atmos.* **129**, e2023JD040667 (2024).
25. Perovich, D. Light reflection and transmission by a temperate snow cover. *J. Glaciol.* **53**, 201–210 (2007).
26. Brandt, R. E., Warren, S. G., Worby, A. P. & Grenfell, T. C. Surface albedo of the Antarctic sea ice zone. *J. Clim.* **18**, 3606–3622 (2005).
27. Riihelä, A., Manninen, T. & Laine, V. Observed changes in the albedo of the Arctic sea-ice zone for the period 1982–2009. *Nat. Clim. Change* **3**, 895–898 (2013).
28. Pegau, W. S. & Paulson, C. A. The albedo of Arctic leads in summer. *Ann. Glaciol.* **33**, 221–224 (2001).
29. Boisvert, L., Webster, M., Parker, C. L. & Forbes, R. M. Rainy days in the Arctic. *J. Clim.* **36**, 6855–6878 (2023).
30. Rampal, P., Weiss, J. & Marsan, D. Positive trend in the mean speed and deformation rate of Arctic sea ice, 1979–2007. *J. Geophys. Res.* **114**, C05013 (2009).
31. Clancy, R., Bitz, C. M., Blanchard-Wrigglesworth, E., McGraw, M. C. & Cavallo, S. M. A cyclone-centered perspective on the drivers of asymmetric patterns in the atmosphere and sea ice during Arctic cyclones. *J. Clim.* **35**, 73–89 (2022).
32. Rogers, J. C. Patterns of low-frequency monthly sea level pressure variability (1899–1986) and associated wave cyclone frequencies. *J. Clim.* **3**, 1364–1379 (1990).
33. Clark, M. P., Serreze, M. C. & Robinson, D. A. Atmospheric controls on Eurasian snow extent. *Int. J. Climatol.* **19**, 27–40 (1999).
34. Zhang, X., Walsh, J. E., Zhang, J., Bhatt, U. & Ikeda, M. Climatology and interannual variability of arctic cyclone activity: 1948–2002. *J. Clim.* **17**, 2300–2317 (2004).
35. Simmonds, I., Burke, C. & Keay, K. Arctic climate change as manifest in cyclone behavior. *J. Clim.* **21**, 5777–5796 (2008).
36. Meier, W. N. et al. *NOAA Arctic Report Card 2023: Sea Ice. NOAA Technical Report OAR ARC; 23-06* (eds Druckenmiller, M. L. et al.) 39–48 (NOAA, 2023); https://doi.org/10.25923/f5t4-b865
37. Screen, J. A. & Simmonds, I. Declining summer snowfall in the Arctic: causes, impacts and feedbacks. *Clim. Dyn.* **38**, 2243–2256 (2012).
38. Neu, U. et al. IMILAST: a community effort to intercompare extratropical cyclone detection and tracking algorithms. *Bull. Am. Meteorol. Soc.* **94**, 529–547 (2013).
39. Environmental Working Group. Environmental Working Group Arctic Meteorology and Climate Atlas, version 1. *National Snow and Ice Data Center* https://doi.org/10.7265/N5MS3QNJ (2000).
40. Perovich, D., Richter-Menge J. & Polashenski C., Observing and understanding climate change: monitoring the mass balance, motion, and thickness of Arctic sea ice. *The CRREL-Dartmouth Mass Balance Buoy Program* http://imb-crrel-dartmouth.org (2024).
41. Ballinger, T. J. et al. *NOAA Arctic Report Card 2023: Surface Air Temperature. NOAA Technical Report OAR ARC; 23-02* (eds Thoman, R. L. et al.) 9–14 (NOAA, 2023); https://doi.org/10.25923/x3ta-6e63
42. Notz, D., SIMIP Community. Arctic sea ice in CMIP6. *Geophys. Res. Lett.* **47**, e2019GL086749 (2020).
43. Jahn, A., Holland, M. M. & Kay, J. E. Projections of an ice-free Arctic Ocean. *Nat. Rev. Earth Environ.* **5**, 164–176 (2024).

Methods

To investigate the relationship between the AO and summertime snow on Arctic sea ice, we use regression, composite and principal component techniques on reanalysis, model and satellite data. While the summer melt season in the Arctic Ocean tends to comprise May–September[44], we placed emphasis on the June–August months, since they represent peak insolation and melt. All data were averaged to monthly values, and anomalies were computed and detrended on the basis of the 1980–2020 mean. Excluding the albedo dataset, anomalies were weighted by the square root of the cosine of latitude for determining principal components.

Correlation maps with statistical significance corresponding to those in in Figs. 1b, 3b, 4b and 6b are available in Extended Data Fig. 1. Regressions of a given variable onto the AO index (or onto the first principal component) were linear. We refer to the first principal component as the leading pattern of variability. We applied composite techniques to investigate the linearity of a given variable's response to the AO. The linear response is defined as the difference between the positive and negative composites, whereas the nonlinear response was defined as the sum of the positive and negative composites, following refs. 45,46. Composites were determined using the extreme 5 years that exceeded one standard deviation of the mean. The interpretation of a linear response is that a variable changes in an equal and opposite manner based on whether the AO phase is positive or negative. For a nonlinear response, a variable changes in the same manner, regardless of the sign of the AO phase.

We performed lead-lag correlations to better understand the relationship between sea-ice coverage, melt–freeze onset timing, pre-existing snow and summer snow depth variability from the perspective of preconditioning. We also correlated the former variables' first principal components against the leading mode in monthly snow depth anomalies. A Bayesian time series decomposition method developed by Zhao et al.[47] was applied to the 1980–2020 June–August SIC time series to identify a breakpoint in 2007. The breakpoint represents an abrupt shift in the sea-ice concentration trend (Extended Data Fig. 8) using a polynomial fit model. The model fit yields a root mean square error of 0.7% and a correlation coefficient of 0.85. The code is freely available at https://github.com/zhaokg/Rbeast.

ERA5 reanalysis

We used the fifth generation of the European Centre for Medium Range Weather Forecasts Reanalysis (ERA5)[48] for investigating the spatiotemporal patterns of 1,000 hPa geopotential height, SLP, 2 m air temperature and snowfall. We computed monthly averages from 6 hour timesteps. The monthly AO indices were constructed following refs. 49,50. Previous works[51–53] have shown that this definition successfully captures summertime atmospheric variability associated with blocking anticyclones, whereas the AO definition of Thompson and Wallace[20] mainly reflects wintertime atmospheric variability. We applied empirical orthogonal function analysis on the temporal covariance matrix of monthly geopotential height fields using a zonally averaged, monthly geopotential height field from 1,000 hPa to 200 hPa north of 40° N. The seasonal cycle was removed from the monthly mean height field. The covariance matrix was used in the empirical orthogonal function analysis, and the gridded data were correspondingly weighted by the square root of the cosine of latitude. The time series were standardized by removing the long-term mean and dividing by the standard deviation of the monthly index. We note that the summer AO trends over 1979–2022 and 1950–2022 are not significant, despite a positive trend in the winter AO (for example, ref. 54).

SnowModel-LG snow depth

SnowModel-LG[55] output was used to investigate snow depth variability over 1980–2020. The model provides snow depth estimates at 25 km × 25 km resolution at daily time steps year round by simulating the surface energy and snow mass budgets in a Lagrangian framework. For consistency in this study, we use the model results forced by ERA5 reanalysis[48]. Snowfall, rainfall, sublimation, blowing snow, snow melt, snow density evolution, superimposed ice, ice dynamics and heat flux are parameterized processes in the model.

The assessment of the SnowModel-LG performance in summer is understudied (for example, ref. 24), and in general, reanalysis-based models for snow on sea ice are difficult to assess due to the dearth of observations and the challenges plaguing remote sensing retrievals (for example, ref. 56). Nevertheless, we evaluated the SnowModel-LG output against ice mass balance buoy data from 1993–2017 (ref. 40) and found that the model underestimates summer snow accumulation by ~27% across the Kara, central Arctic and Beaufort regions. The low bias is a known issue in other seasons, and accordingly, the precipitation forcing is scaled by a factor greater than one[57]. In further comparison with historical observations[13], the springtime standard deviation in simulated snow depth ranges regionally from 3 cm (Greenland Sea) to 6 cm (Kara Sea), whereas historical observations from the central Arctic yield 6 cm. Even with the scaled precipitation, the low bias still persists, which may affect the correlations between summer snow depth variability and the AO.

Regarding sea-ice drift, in ref. 58, a comparison between the ice motion product used in SnowModel-LG and ice mass buoys revealed a slow bias in the ice motion data, particularly in the East Greenland Sea. Such a bias probably amplifies the spatial correspondence between cyclone-associated snowfall and simulated snow depth anomalies in areas with rapid ice drift. Given that sea ice moves on the order of 6 km per day in June–August[30], we expect there to be a small effect on the regional results presented in this work, particularly in the Fram Strait region where summer ice drift is largest. More details on the model physics in SnowModel-LG can be found in ref. 57.

Snow depth observations

We use snow observations from the 1954–1991 North Pole drifting ice stations[39] and ice mass balance buoys from 1993–2017 (ref. 40) for corroborating results from the SnowModel-LG analysis. Snow sampling at the drifting ice stations continued in summer as long as one of the following criteria was met: snow covered 50% of the transect line or the average snow depth on the transect line was at least 5 cm (ref. 13). Snow depth from the ice mass balance buoys was derived from downward-looking sonic rangefinders and has a reported accuracy of 1 cm.

Cyclones

Closed cyclone systems were identified using the Melbourne University cyclone tracking scheme[35,59–61] applied to 6 hourly SLP fields from ERA5 reanalysis. We refer readers to the references above for more details and briefly describe the methodology here. SLP fields were converted to polar stereographic coordinates and interpolated to a one-latitudinal grid using a bicubic spline. The Laplacian of the SLP fields was used to determine the local maxima relative to eight neighbouring grid cells. Closed cyclone systems were identified when the local maxima met the following criteria: the second derivative of the SLP was positive in the x and y directions, and the mean Laplacian in the immediate vicinity of the maximum was equal to or greater than 0.2 hPa per square degree. We fit an ellipse to the first and second derivatives of the SLP fields to identify the cyclone area. While the Melbourne University cyclone tracking scheme identifies both open and closed systems, only closed cyclone systems were used in this analysis due to the ill-defined boundaries of open systems. We evaluated the number of days that cyclones were present in each grid cell per month, and these are defined as 'cyclones' hereafter. For cyclone intensity, we examined the minimum SLP within the cyclone area.

Satellite retrievals of SIC, melt-freeze dates and albedo

Four types of satellite retrievals were used in the analysis: SIC, melt–freeze onset dates, surface albedo and melt ponds. For SIC, we use Ocean and Sea Ice Satellite Applications Facility (OSI SAF) OSI-450-monthly global SIC climate data record, release 3 (ref. 62), which is produced at 25 km resolution. For summertime retrievals, the retrieval errors can be more than 20% from the effects of weather and melt ponding on brightness temperatures[63], but their influence on trends in sea-ice area and extent is generally considered to be small[64]. For the melt and freeze onset dates, we used the passive microwave melt product developed by Markus et al.[65]. The first dates of continuous melt and freeze were incorporated into the analysis.

For surface albedo, we use satellite-based estimates from the third edition of the Satellite Application Facility on Climate Monitoring Clouds, Albedo and Radiation (CLARA) Climate Data Record[66]. The CLARA-A3 record is based on intercalibrated Advanced Very High Resolution Radiometer data spanning 1979–2020 for the Climate Data Record component, which is used here. The albedo data in CLARA-A3 have been evaluated against a wide array of reference in situ observations and benchmarked against other similar satellite data records; the mean retrieval bias over the cryospheric domain, inclusive of sea ice, is evaluated at 10–15% (relative). The retrievals have been shown to be capable of tracking the albedo decrease of the sea ice during the melting season. The monthly mean blue-sky albedo estimates for July were selected and filtered with OSI SAF OSI-450-a SIC data[62] to contain only the continuous sea-ice zone, that is, the area where ice concentration is larger than 80%. Then, continuous ice grid cells, where the albedo estimate was based on less than 100 Advanced Very High Resolution Radiometer-Global Area Coverage observations, were discarded to ensure sufficient sampling for robust estimation. Note that by 2020, the continuous sea-ice zone in July shrank to approximately two-thirds of its early 1980s areal coverage. Nonetheless, the ice-covered area remained large enough to reliably investigate the effect of enhanced snowfall on the mean surface albedo of sea ice. July albedos were selected in the comparison with the June–July AO based on two findings from the analysis: (1) May snow conditions have minimal effect on July snow depth variability but a noteworthy impact on June snow depth variability, and (2) the freeze-up timing affects August snow depth variability. Thus, July is a representative month for comparison of peak summer melt conditions, surface albedo and the AO.

We obtained spatially resolved MODIS-Peng (NENU-MPF) melt pond fraction (MPF) data for 2000–2020 from ref. 67, and nearest neighbour resampled it to the CLARA grid as monthly means and used it to remove the mean melt pond impact on July surface albedo. Due to a sizable pole hole in the MPF data product, this was done by deriving a mean linear relationship between MPFs and CLARA albedo in July from all valid grid cell data ($N = 125,422$, $r = −0.20$, $P = 0$) and applying the slope (delta-albedo $−0.326 \times$ MPF) with the Arctic-wide mean July MPF to correct for melt pond albedo effects in the mean July sea-ice albedo.

Data availability

SnowModel-LG data are available via the National Snow and Ice Data Center at https://doi.org/10.5067/27A0P5M6LZBI. The CLARA-A3 surface albedo data are available at https://doi.org/10.5676/EUM_SAF_CM/CLARA_AVHRR/V003. ERA5 reanalysis data are available via Copernicus Climate Change Service Climate Data Store at https://doi.org/10.24381/cds.adbb2d47. Melt onset and freeze-up dates are available on the Goddard Space Flight Center website at https://earth.gsfc.nasa.gov/cryo/data/arctic-sea-ice-melt. MPFs are available via Zenodo at https://zenodo.org/records/6888170 (ref. 68). The North Pole drifting ice station data are available at https://doi.org/10.7265/N5MS3QNJ. The ice mass balance buoy data are available at https://imb-crrel-dartmouth.org/results/. The OSI SAF sea ice concentration data are available at https://osi-saf.eumetsat.int/products/osi-450.

Code availability

While not used for the analysis, we point interested parties in the University of Melbourne cyclone detection and tracking algorithm[59] to the following website for the cyclone tracker code at https://cyclonetracker.earthsci.unimelb.edu.au/. We refer interested parties in the Bayesian breakpoint methodology to the following website for downloading the code: https://doi.org/10.1016/j.rse.2019.04.034. The code for creating stereographic maps was developed by Andrew Roberts and is available at https://www.mathworks.com/matlabcentral/fileexchange/30414-ncpolarm, while the basemap information is provided in the Matlab Mapping Toolbox dataset.

References

44. Peng, G., Steele, M., Bliss, A. C., Meier, W. N. & Dickinson, S. Temporal means and variability of arctic sea ice melt and freeze season climate indicators using a satellite climate data record. *Remote Sensing* **10**, 1328 (2018).
45. Deweaver, E. & Nigam, S. Linearity in ENSO's atmospheric response. *J. Climate* **15**, 2446–2461 (2002).
46. Simpkins, G. R., Ciastro, L. M., Thompson, D. W. J. & England, M. H. Seasonal relationships between large-scale climate variability and Antarctic sea ice concentration. *J. Clim.* **25**, 5451–5469 (2012).
47. Zhao, K. et al. Detecting change-point, trend, and seasonality in satellite time series data to track abrupt changes and nonlinear dynamics: a Bayesian ensemble algorithm. *Remote Sens. Environ.* **232**, 111181 (2019).
48. Hersbach, H. et al. ERA5 hourly data on single levels from 1979 to present. *Copernicus Clim. Change Serv. Clim. Data Store* https://doi.org/10.24381/cds.adbb2d47 (2018).
49. Ogi, M., Yamazaki, K. & Tachibana, Y. The summertime annular mode in the Northern Hemisphere and its linkage to the winter mode. *J. Geophys. Res. Atmos.* **109**, D20114 (2004).
50. Ogi, M., Rysgaard, S. & Barber, D. G. Importance of combined winter and summer Arctic Oscillation (AO) on September sea ice extent. *Environ. Res. Lett.* **11**, 034019 (2016).
51. Ogi, M., Yamazaki, K. & Tachibana, Y. The summer northern annular mode and abnormal summer weather in 2003. *Geophys. Res. Lett.* **32**, L04706 (2005).
52. Tachibana, Y., Nakamura, T., Komiya, H. & Takahashi, M. Abrupt evolution of the summer Northern Hemisphere annular mode and its association with blocking. *J. Geophys. Res.* **115**, D12125 (2010).
53. Otomi, Y., Tachibana, Y. & Nakamura, T. A possible cause of the AO polarity reversal from winter to summer in 2010 and its relation to hemispheric extreme summer weather. *Clim. Dyn.* **40**, 1939–1947 (2013).
54. Jeong, Y. C., Yeh, S. W., Lim, Y. K., Santoso, A. & Wang, G. Indian Ocean warming as key driver of long-term positive trend of Arctic Oscillation. *npj Clim. Atmos. Sci.* **5**, 56 (2022).
55. Liston, G. E., Stroeve, J. & Itkin, P. Lagrangian snow distributions for sea-ice applications, version 1. *NASA National Snow and Ice Data Center Distributed Active Archive Center* https://doi.org/10.5067/27A0P5M6LZBI (2021).
56. Zhou, L. et al. Inter-comparison of snow depth over Arctic sea ice from reanalysis reconstructions and satellite retrieval. *The Cryosphere* **15**, 345–367 (2021).
57. Liston, G. E. et al. A Lagrangian snow-evolution system for sea-ice applications (SnowModel-LG): part I—model description. *J. Geophys. Res. Oceans* **125**, e2019JC015913 (2020).
58. Horvath, S. et al. A database for investigating the fate of Arctic sea ice and interaction with the polar atmosphere in a Lagrangian framework. *Sci. Data* **10**, 73 (2023).
59. Murray, R. J. & Simmonds, I. A numerical scheme for tracking cyclone centres from digital data. Part I: development and operation of the scheme. *Aust. Meteor. Mag.* **39**, 155–166 (1991).

60. Sinclair, M. R. Objective identification of cyclones and their circulation intensity, and climatology. *Weather Forecast.* **12**, 595–612 (1997).

61. Lim, E.-P. & Simmonds, I. Southern Hemisphere winter extratropical cyclone characteristics and vertical organization observed with the ERA-40 reanalysis data in 1979–2001. *J. Clim.* **20**, 2675–2690 (2007).

62. OSI SAF global sea ice concentration climate data record 1978–2020, v3.0, OSI-450-a. *EUMETSAT Ocean and Sea Ice Satellite Application Facility* https://doi.org/10.15770/EUM_SAF_OSI_0013 (2022).

63. Kern, S., Lavergne, T., Notz, D., Pedersen, L. T. & Tonboe, R. T. Satellite passive microwave sea-ice concentration data set intercomparison for Arctic summer conditions. *Cryosphere Discuss.* **17**, 2469–2493 (2020).

64. Andersen, S., Tonboe, R., Kaleschke, L., Heygster, G. & Pedersen, L. T. Intercomparison of passive microwave sea ice concentration retrievals over the high-concentration Arctic sea ice. *J. Geophys. Res.* **112**, C08004 (2007).

65. Markus, T., Stroeve, J. C. & Miller, J. Recent changes in Arctic sea ice melt onset, freezeup, and melt season length. *J. Geophys. Res.* **114**, C12024 (2009).

66. Riihelä, A., Jääskeläinen, E. & Kallio-Myers, V. Four decades of global surface albedo estimates in the third edition of the CLARA climate data record Earth Syst. *Sci. Data* **16**, 1007–1028 (2024).

67. Peng, Z., Ding, Y., Qu, Y., Wang, M. & Li, X. Generating a long-term spatiotemporally continuous melt pond fraction dataset for arctic sea ice using an artificial neural network and a statistical-based temporal filter. *Remote Sens.* **14**, 4538 (2022).

68. Qu, Y. NENU-MPF dataset. *Zenodo* https://zenodo.org/records/6888170 (2022).

Acknowledgements

Author contributions

M.A.W. led the conception, data collection, analysis and writing. A.R. contributed to the data collection, analysis and writing. All authors contributed to the interpretation of the results and edited the paper.

Competing interests

The authors declare no competing interests.

Additional information

Extended data is available for this paper at https://doi.org/10.1038/s41561-024-01525-y.
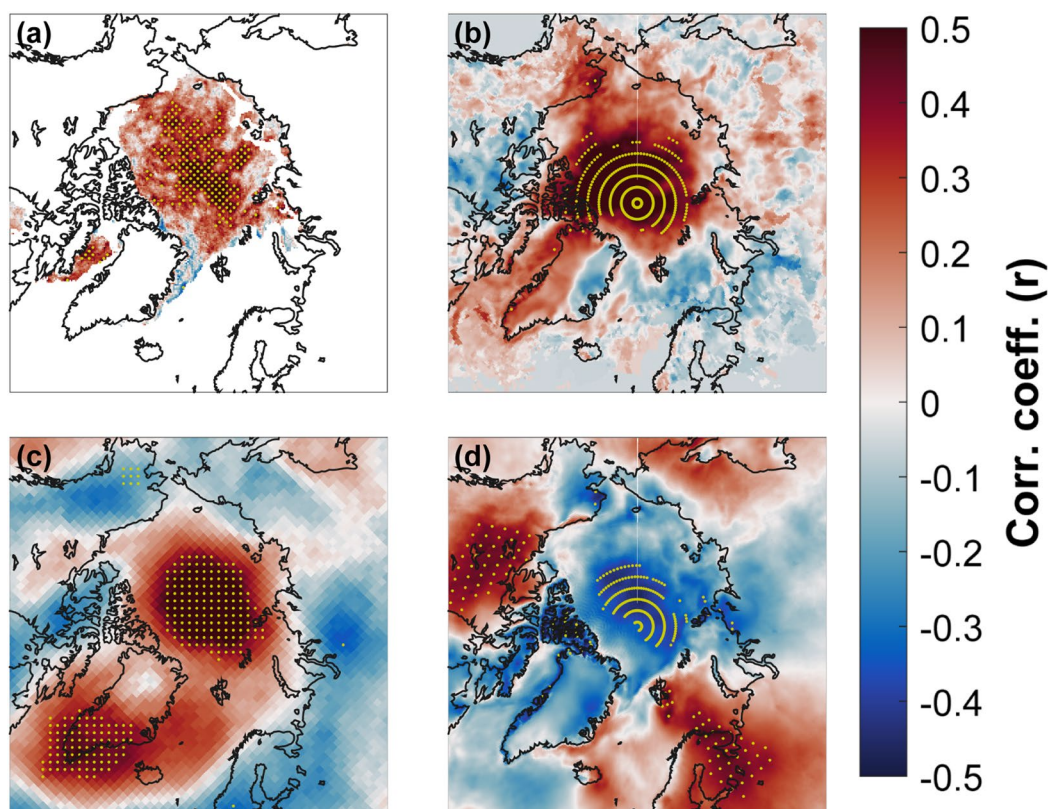
Correspondence and requests for materials should be addressed to Melinda A. Webster.

Peer review information *Nature Geoscience* thanks Jack C. Landy and the other, anonymous, reviewer(s) for their contribution to the peer review of this work. Primary Handling Editor: James Super, in collaboration with the *Nature Geoscience* team.

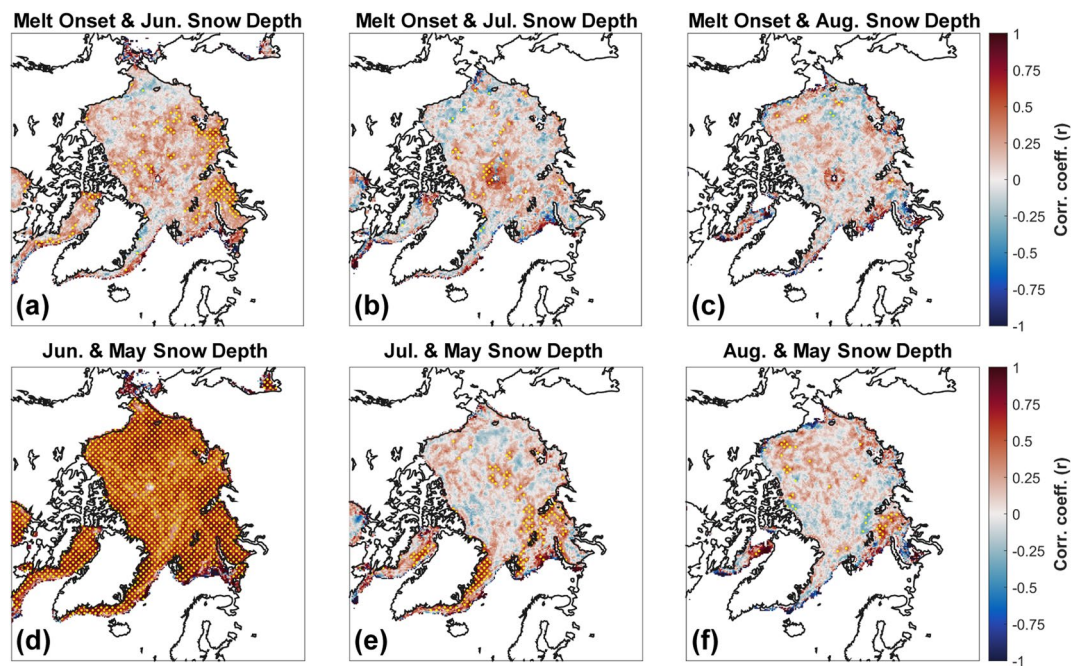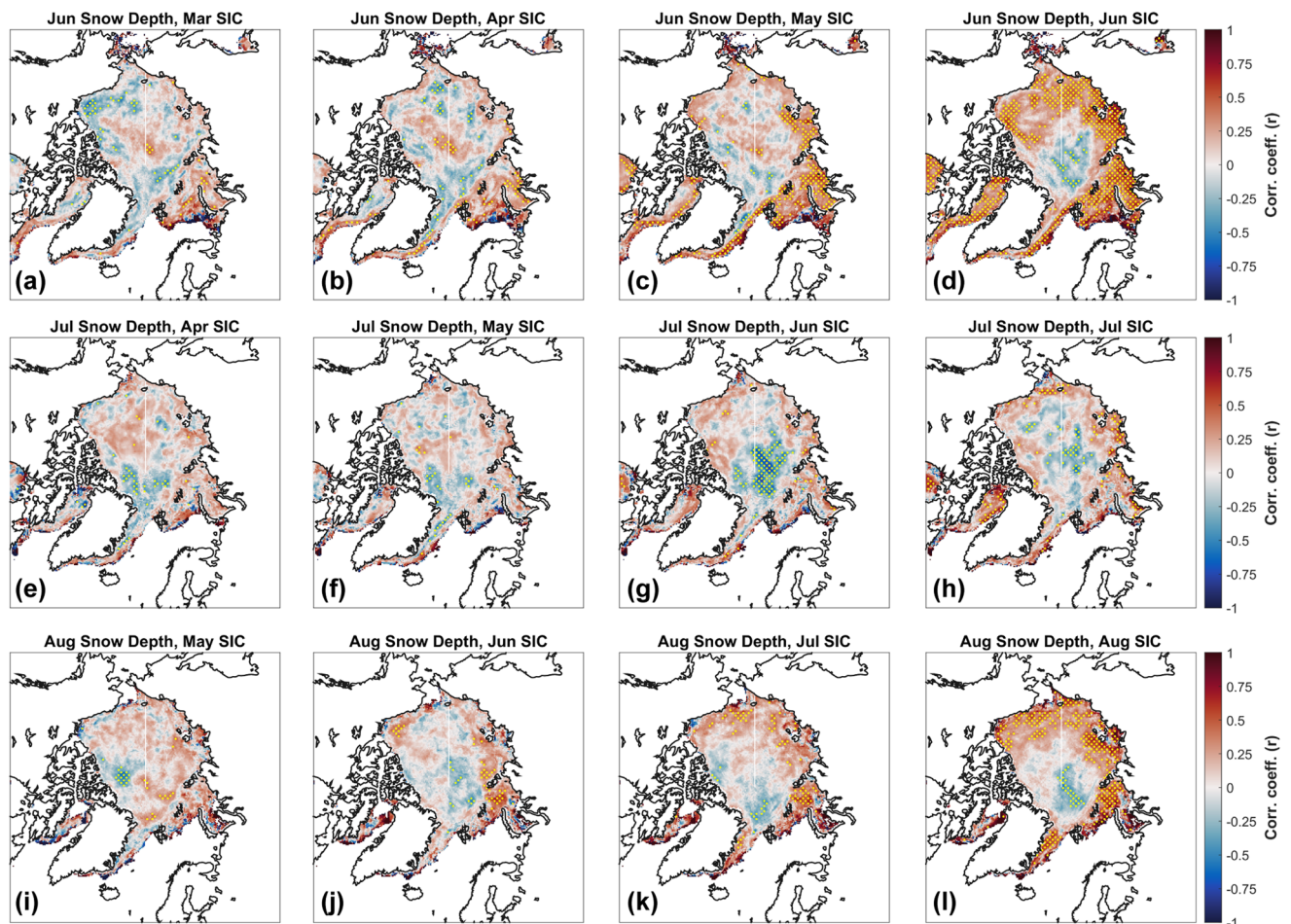**Reprints and permissions information** is available at www.nature.com/reprints.

Extended Data Fig. 1 | Correlations and statistical significance between the Arctic Oscillation and different environmental variables. The June-August mean correlations for 1980–2020 between the Arctic Oscillation and **(a)** snow depth anomalies, **(b)** snowfall anomalies, **(c)** anomalies of the daily presence of cyclones, and **(d)** 2 m air temperature anomalies. The yellow dots indicate correlations with 95% statistical significance. Note that the different spatial resolutions between data products yield different spacing between yellow dots of statistical significance across the panels.
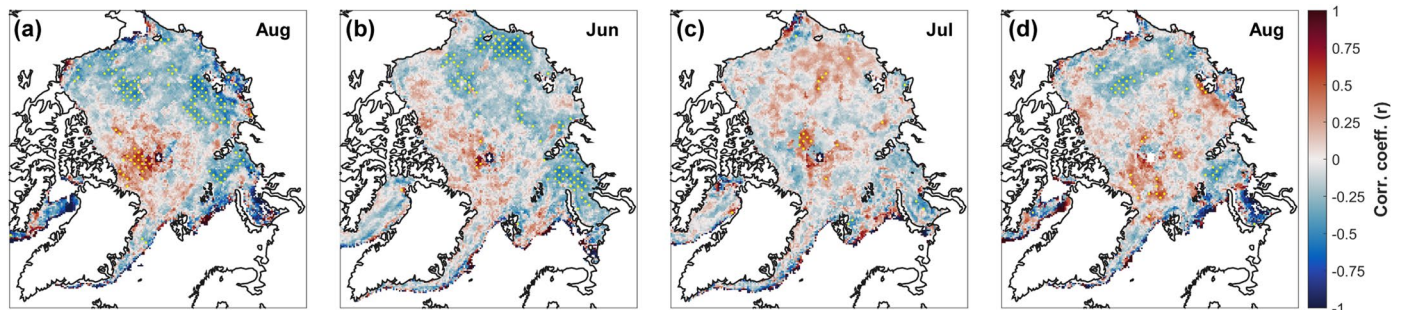
Extended Data Fig. 2 | Correlations and statistical significance between snow depth across different months and timing of melt onset. Correlation coefficients of anomalies for 1980–2020 between: the date of melt onset and **(a)** June, **(b)** July, and **(c)** August snow depths; May snow depths and **(d)** June, **(e)** July, and **(f)** August snow depths. 95% statistical significance is marked by yellow dots. Equivalent figure in the main text is Fig. 3.
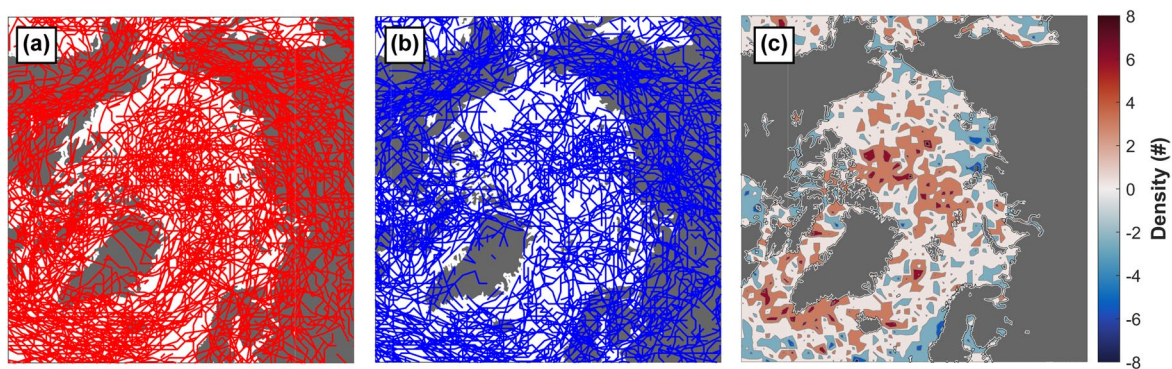
Extended Data Fig. 3 | Correlations and statistical significance between monthly snow depth and sea ice concentration. Correlation coefficients of anomalies between **(a-d)** June snow depths and sea ice concentrations in months prior to June, **(e-h)** July snow depths and sea ice concentrations in months prior to July, and **(i-l)** August snow depths and sea ice concentrations in months prior to August. 95% statistical significance is marked by yellow dots.
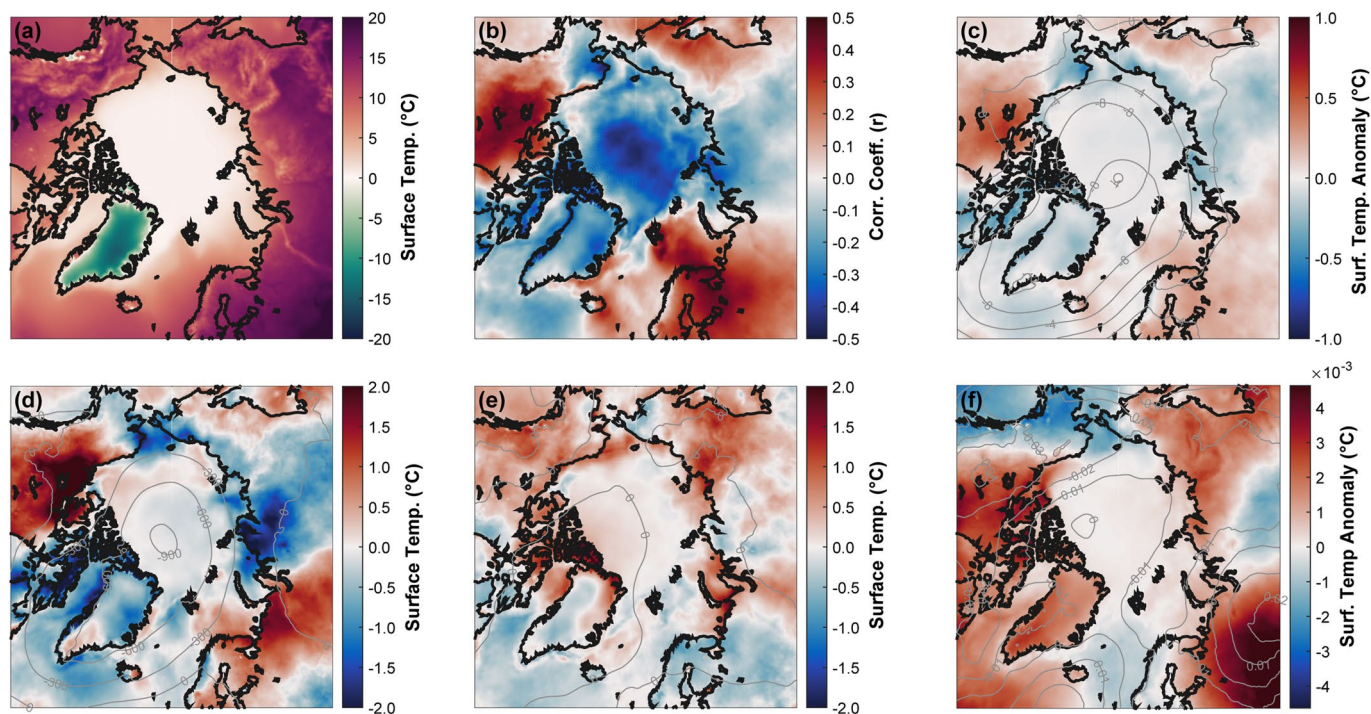
Extended Data Fig. 4 | Correlations and statistical significance between snow depth and sea-ice freeze-up timing. (a) Correlations between the same year's freeze-up and August snow depth anomalies. **(b)** Correlations between the previous year's freeze-up and June snow depth anomalies. **(c)** Correlations between the previous year's freeze-up and July snow depth anomalies. **(d)** Correlations between the previous year's freeze-up and August snow depth anomalies. Areas with 95% statistical significance are indicated by yellow dots.
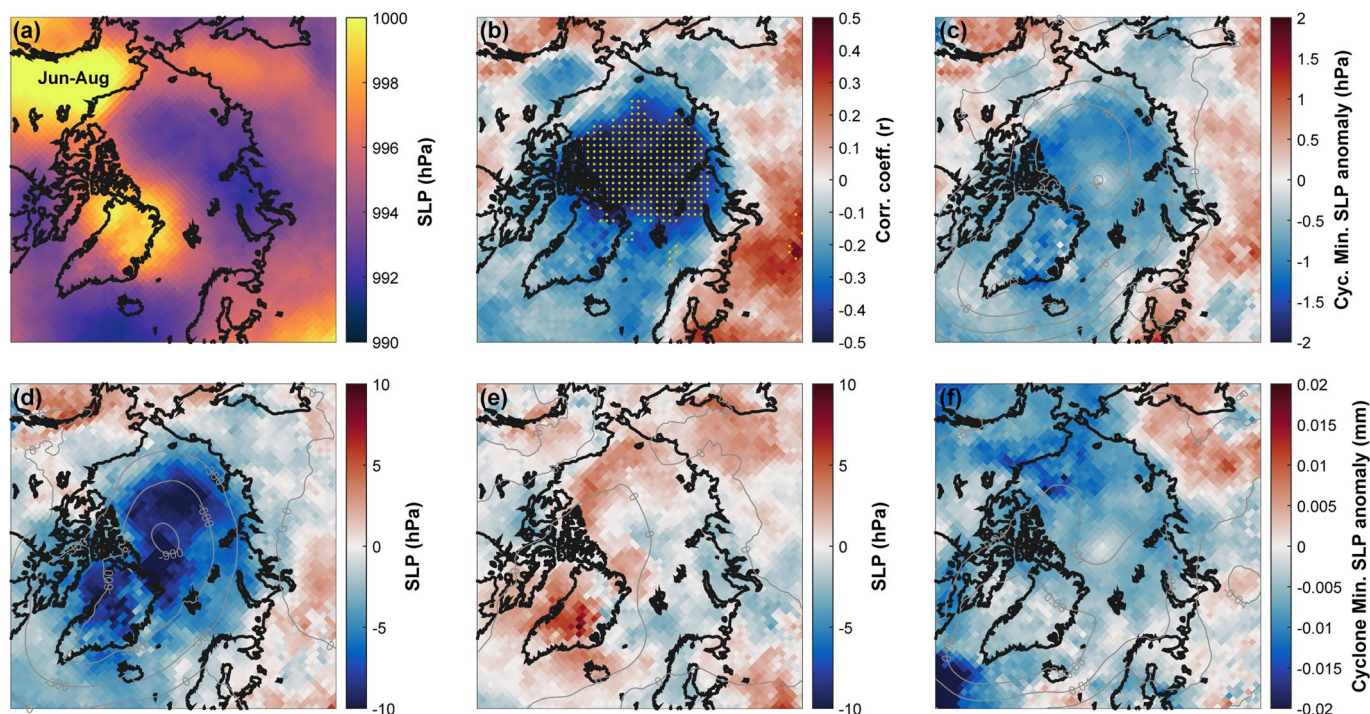
Extended Data Fig. 5 | Cyclone tracks and the cyclone track density difference between five years with the most extreme positive and negative Arctic Oscillation index. (**a**) Cyclone tracks for the five years with the most positive Arctic Oscillation index in June-August. (**b**) Cyclone tracks for the five years with the most negative Arctic Oscillation index in June-August. (**c**) The difference in cyclone track densities of unique cyclones between the five most extreme positive and negative Arctic Oscillation years for June-August. The density difference north of 80°N was 99% statistically different using a standard t-test.
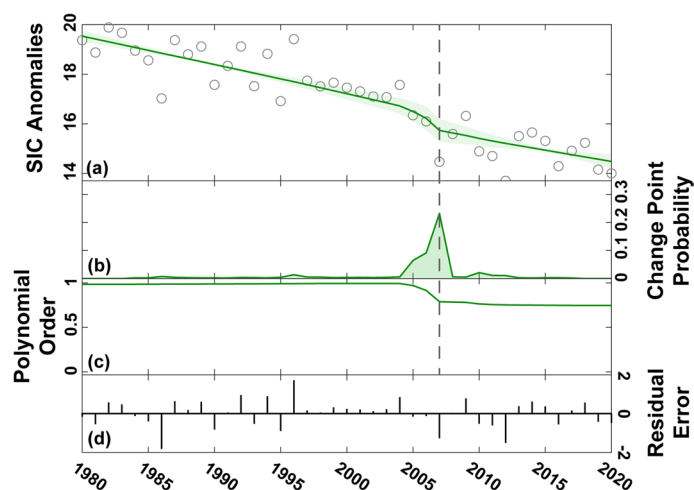
Extended Data Fig. 6 | The climatology and relationship of 2-meter air temperature with the Arctic Oscillation. The June-August mean for 1980–2020 in (**a**) 2 m air temperatures, (**b**) the correlation between 2 m air temperature anomalies and the Arctic Oscillation, (**c**) 2 m air temperature anomalies regressed onto the Arctic Oscillation index, (**d**) the linear response (composite difference) in 2 m air temperature anomalies to the Arctic Oscillation, (**e**) the nonlinear response (composite sum) in 2 m air temperature anomalies to the Arctic Oscillation, and (**f**) 2 m air temperature anomalies regressed onto the first principal component of 2 m air temperatures. The light grey contours in panels (**c**)-(**f**) are the corresponding results using 1000-hPa geopotential height anomalies.
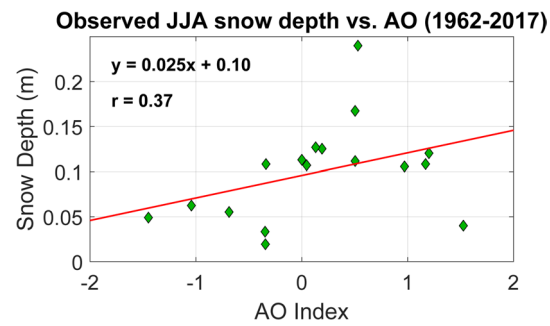
Extended Data Fig. 7 | The climatology and relationship of the minimum sea level pressure within cyclones and the Arctic Oscillation. The June-August mean for 1980–2020 in **(a)** the minimum sea level pressure (SLP) within cyclones, **(b)** the correlation between cyclone SLP anomalies and the Arctic Oscillation with yellow dots indicating correlations with 95% statistical significance, **(c)** cyclone SLP anomalies regressed onto the Arctic Oscillation index, **(d)** the linear response (composite difference) in cyclone SLP anomalies to the Arctic Oscillation, **(e)** the nonlinear response (composite sum) in cyclone SLP anomalies to the Arctic Oscillation, and **(f)** cyclone SLP anomalies regressed onto the first principal component of cyclones. The light grey contours in panels (c)-(f) are the corresponding results using 1000-hPa geopotential height anomalies.

Extended Data Fig. 8 | The time-series breakpoint in June-August sea ice concentration. **(a)** The trend (bold green line) in the June-August sea ice concentration (SIC) anomalies, in percentage, based on the 1980–2020 mean. The time-series break point is denoted by the vertical dashed line. Anomalies are represented by grey hollow circles and the light green shading denotes the 95% confidence interval. The trend is determined from a piece-wise polynomial model. **(b)** The probability (bold green line) of the break point within the time-series, with the time-series break point denoted by the vertical dashed line. **(c)** The polynomial order of the best fit line to the SIC anomaly time-series, with the time-series break point denoted by the vertical dashed line. **(d)** The residual error of the Bayesian model fitted to the SIC anomaly time-series, in percentage.

Extended Data Fig. 9 | The linear fit between mean Arctic snow depths and the Arctic Oscillation index. The June-August average snow depths and Arctic Oscillation (AO) indices from the North Pole drifting ice stations and ice mass balance buoys for the 1962, 1970, and 1994–2017 period. The correlation is statistically significant to 86%.